

EI: Early Intervention for Multimodal Imaging based Disease Recognition

Qijie Wei Hailan Lin Xirong Li*

Renmin University of China

Beijing Key Laboratory for Intelligent Diagnosis of Fundus Diseases and Drug-Device R&D and Translation

<https://github.com/ruc-aimc-lab/EI>

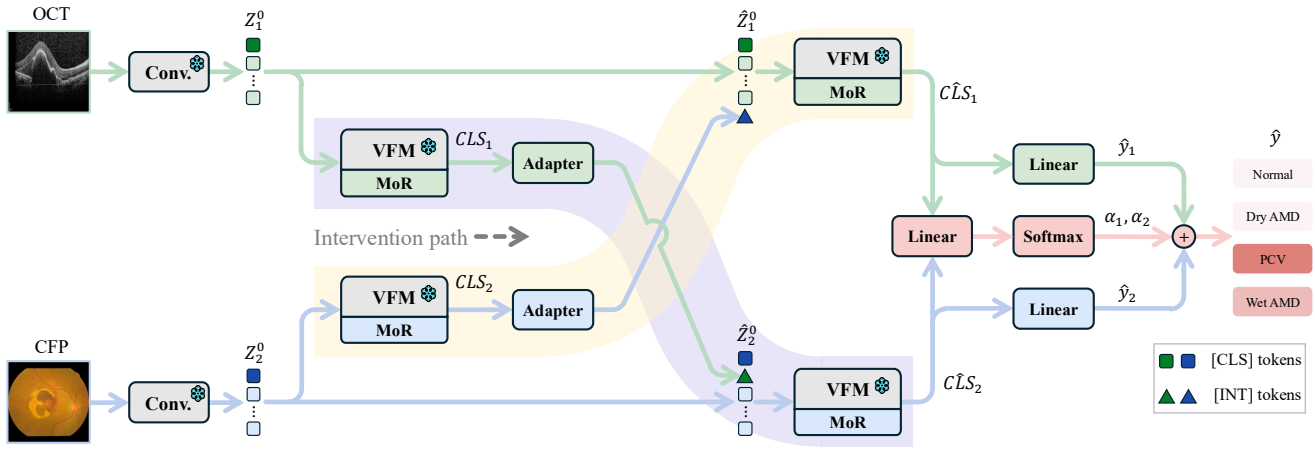


Figure 1. **Proposed Early Intervention (EI) framework for multimodal imaging based disease recognition.** Given a multimodal image sample (an OCT and a CFP in the showcase), each modality is designated in sequence as a *target* modality, with the rest as its *reference*. EI utilizes the high-level semantics encapsulated in the [CLS] tokens from the reference as **intervention** ([INT]) tokens to guide the target-modality feature extraction at an *early* stage. Such a design mirrors a clinician’s typical workflow, where an initial interpretation of one modality contextually informs the examination of another. Moreover, we develop **Mixture of Low-varied-Ranks Adaptation (MoR)** for parameter-efficient adaptation of Vision Foundation Models (VFMs) to medical images. Our framework works for multiple tasks including retinal disease recognition, skin lesion recognition, and knee anomaly classification.

Abstract

Current methods for multimodal medical imaging based disease recognition face two major challenges. First, the prevailing “fusion after unimodal image embedding” paradigm cannot fully leverage the complementary and correlated information in the multimodal data. Second, the scarcity of labeled multimodal medical images, coupled with their significant domain shift from natural images, hinders the use of cutting-edge Vision Foundation Models (VFMs) for medical image embedding. To jointly address the challenges, we propose a novel **Early Intervention (EI)** framework. Treating one modality as target and the rest as reference, EI harnesses high-level semantic tokens from the reference as **intervention tokens** to steer the target modality’s embedding process at an early stage. Further-

more, we introduce **Mixture of Low-varied-Ranks Adaptation (MoR)**, a parameter-efficient fine-tuning method that employs a set of low-rank adapters with varied ranks and a weight-relaxed router for VFM adaptation. Extensive experiments on three public datasets for retinal disease, skin lesion, and knee anomaly classification verify the effectiveness of the proposed method against a number of competitive baselines.

1. Introduction

Multimodal medical imaging is vital in modern healthcare, providing objective clinical profiles by visualizing organs through complementary devices and viewpoints [8]. Recognizing diseases from such multimodal image data is therefore an important task in computer vision. In this paper, we tackle the task with a novel Vision Foundation Model

* Corresponding author: Xirong Li (xirong@ruc.edu.cn)

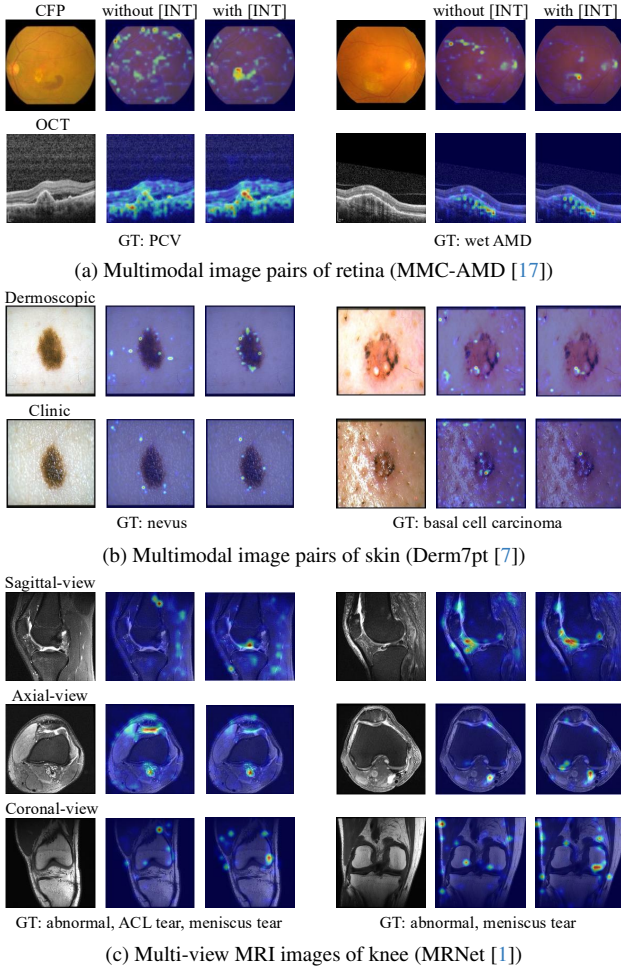


Figure 2. **Multimodal medical images and their patch-level similarity maps w.r.t. the [CLS] token.** VFM: DINOv2. As [CLS] is used for classification, such maps reflect patch-wise contributions to the final prediction. Per target modality (say CFP), the inclusion of the [INT] token from its reference modality (say OCT) leads to more *lesion*-focused maps. Best viewed in color.

(VFM) based method, see Fig. 1.

Each modality in a multimodal image sample provides unique and complementary information. In fundus imaging, for instance (Fig. 2a), Color Fundus Photography (CFP) captures the *en face* of the retina, showing vessels, the optic disc, and the macula, while Optical Coherence Tomography (OCT) reveals the retina’s cross-sectional structure [10]. How to effectively extract and fuse discriminative features from the multimodal sample is crucial for generating embeddings useful for retinal disease recognition.

Existing methods, say MM-MIL [10] for retinal disease recognition, CosCatNet [25] for skin lesion classification and RadDiag [23] for radiology-based disease diagnosis, generate the embeddings in a two-step manner. Firstly, unimodal image embedding (UIE) is performed with modality-

Table 1. **Current methods for multimodal imaging based disease (lesion) recognition.** Different from the prior works, our Early Intervention (EI) method provides cross-modal guidance *before* unimodal image embedding (UIE) and *MoR* as an enhanced mixture of LoRAs for parameter-efficient fine-tuning (PEFT) of vision foundation models (VFMs).

Method	UIE	Cross-modal guidance	PEFT	Tasks
MM-MIL[10]	ResNet	After UIE	-	·Retinal disease classification
SFusion[11]	U-Net	After UIE	✗	·Brain tumor segmentation
GeCoM-Net[18]	DenseNet	After UIE	-	·Retinal disease classification
CoscatNet[25]	ResNet	After UIE	-	·Skin lesion recognition
RadDiag[23]	ResNet+ViT	After UIE	✗	·Radiology based diagnosis
MMRAD[9]	VFM	After UIE	Prompt	·Retinal anomaly detection
Proposed EI	VFM	<i>Before</i> UIE	MoR	·Retinal disease classification ·Skin lesion recognition ·Knee anomaly classification

specific vision encoders to extract features per modality. These unimodal features are then fused via vector concatenation [25], weighted summation [10] or self attention [23] to produce a joint representation. Despite their varied fusion strategies, these methods have a common pattern: **fusion after UIE**, see Tab. 1.

We argue that introducing cross-modal guidance after UIE may be too late to fully leverage the complementary and correlated information in the multimodal data. In fact, such a delayed inter-modal interaction is misaligned with clinical practice, where a clinician rarely interpret modalities in isolation. Instead, they often form an initial hypothesis from one modality and use it to contextually guide the interpretation of another. We identify the delayed fusion paradigm as a key bottleneck in advancing multimodal imaging based disease recognition.

For learning effective multimodal medical image embeddings, innovating the fusion paradigm alone is insufficient. Given the scarcity of labeled data in medicine, data-efficient learning algorithms are equally critical. VFMs like CLIP [15] and DINOv2 [14], pre-trained on massive amounts of Internet images, provide powerful representations for natural images. However, the significant domain gap between natural and medical images makes their direct application problematic. As summarized in Tab. 1, existing methods typically rely on full-parameter tuning of ImageNet-pretrained encoders. MMRAD [9] makes an initial attempt to adapt a VFM for retinal anomaly detection using prompt learning. However, as prompt tuning is primarily designed to activate a model’s pre-existing knowledge, it is suboptimal for scenarios requiring the integration of new, task-specific knowledge due to a significant domain shift. How to best leverage cutting-edge VFMs for the current task remains largely unexplored.

In this paper, we propose **Early Intervention (EI)**, a new framework for multimodal medical image embedding that introduces cross-modal guidance *before* UIE. As shown

in Fig. 1, viewing one modality as target and the rest as reference, EI leverages the high-level semantics encapsulated in the [CLS] tokens from reference modalities, extracted by auxiliary VFMs, as “**intervention tokens**” ([INT]) to guide UIE of the target at an early stage. This design mirrors a clinician’s typical workflow, where an initial interpretation of one modality contextually informs the examination of another. As demonstrated in Fig. 2, the inclusion of the [INT] token leads to more *lesion*-focused feature extraction. Furthermore, inspired by the success of LoRA [4] and its Mixture of Experts (MoE) extension LoRAMoE [3], we introduce **Mixture of Low-varied-Ranks Adaptation (MoR)**. The MoR module employs a set of low-rank adapters with different ranks and a relaxed router with a *bypass* (Fig. 3), enabling more effective and parameter-efficient fine-tuning.

In sum, this work makes three contributions as follows:

- **A novel multimodal fusion framework.** The proposed early intervention path (Fig. 1) effectively propagates cross-modal guidance, thereby overcoming the information bottleneck in previous methods caused by the fusion-after-UIE mechanism.
- **A better PEFT method.** Compared to its predecessors (LoRA and LoRAMoE), the proposed MoR employs low-rank adapters with different ranks, enabling more effective adaptation of VFMs to medical images.
- **State-of-the-art performance.** We conduct extensive experiments on three multimodal medical imaging datasets, *i.e.* MMC-AMD [17], Derm7t [7] and MRNet [1], for fundus, skin and knee image classification, respectively. The results consistently show the superiority of the proposed method over a number of competitive baselines.

2. Related Work

Our contributions lie at the intersection of multimodal medical image embedding and parameter-efficient fine-tuning. We therefore review briefly recent progress in these two areas and, accordingly, clarify our novelties.

2.1. Multimodal Medical Image Embedding

Given a multimodal image sample, depending on how its modality-specific embeddings are combined, we categorize existing methods into the following three groups. That is, concatenation [18, 25], weighted summation [10, 11] and attention-based fusion [9, 23].

In the context of skin lesion classification, CosCatNet [25] first uses two ResNets to obtain dermoscopic and clinic image features and then concatenates them to obtain a multimodal embedding. The concatenation operation is also used in GeCoM-Net [18] for multimodal retinal disease recognition. In a similar context, MM-MIL [10] first uses two ResNets in parallel to extract features from given CFP and OCT images, respectively. The resultant features are then weightedly summed up, with the weights determined

by a lightweight multiple instance learning module. Alternatively, SFusion [11] computes the fusion weights with multiple self-attention layers for brain tumor segmentation. Regarding attention-based fusion, RadDiag [23] employs self-attention to integrate embeddings of multimodal radiological images for radiology based long-tailed disease diagnosis. By contrast, MMRAD [9] uses two cross-attention blocks in sequence to fuse embeddings of CFP and OCT images for retinal anomaly detection.

Despite their varied fusion strategies, all existing methods share a common pattern: fusion after unimodal image embedding (UIE), see Tab. 1. UIE is a crucial step, yet uninformed by other modalities. The proposed EI framework tackles this fundamental issue by enabling cross-modal guidance *before* UIE.

2.2. Parameter Efficient Fine-tuning

In order to effectively adapt a given VFM for downstream tasks where labeled samples are in relatively short supply (as in the medical domain), parameter-efficient fine-tuning (PEFT) is crucial. Depending on how the adaptation is achieved, current methods for PEFT can be roughly divided into three categories: prompt learning [6], selective parameter tuning [21], and lightweight plug-ins [4].

In VPT [6], a fixed set of learnable tokens, known as prompts, are prepended to each input sequence. To generate input-dependent prompts, MMRAD [9] improves upon VPT by extracting prompts directly from an input image using a shallow network. While prompt learning aims to activate a model’s pre-existing knowledge, selective parameter tuning explicitly instills task-specific knowledge. For instance, RLRR [2] adjusts each linear layer’s weight matrix using row-wise and column-wise rescaling vectors, whereas BiTFit [21] optimizes only the bias terms. LoRA [13] introduces a plug-in low-rank matrix that operates alongside the original weights in the linear layers. Subsequent methods build on this concept. For instance, LoSA [13] attaches auxiliary adapters to the backbone network to enable more efficient gradient propagation, while LoRAMoE [3] employs a mixture of experts, with multiple low-rank matrices per linear layer. Inspired by the strong performance of the LoRA series [12], we develop MoR, replacing the fixed rank used in prior work with an auto-routed multi-rank strategy.

3. Method

We aim to build a VFM-based medical image classifier that performs C -class disease recognition based on M -modality image input. Let \mathcal{D} be a labeled set of M -modality image samples $\{(x, y)\}$, where $x[i]$ denotes the i -th modality image, $i = 1, \dots, M$, and $y \in \{0, 1\}^C$ is the corresponding label in a C -class setting. In the proposed early intervention (EI) framework, each modality is designated in sequence as a *target* modality, indexed by t , with the rest as its *reference*

denoted as $R = \{1, \dots, M\}/\{t\}$. Thus, all the modalities will alternate between the role of target and reference.

Given ϕ as a pre-trained VFM, we associate each modality with a primary VFM ϕ_p and an auxiliary VFM ϕ_a . The former extracts features for classification when the modality is the target. The latter generates an intervention token ([INT]) when the modality serves as (part of) the reference. Next, we depict the generation of the [INT] token (Sec. 3.1), followed by its use in target-modality feature extraction (Sec. 3.2). Given the features extracted from the M modalities, a lightweight late fusion module is provided in Sec. 3.3. The proposed Mixture of Ranks (MoR) for parameter-efficient VFM adaptation is presented in Sec. 3.4. A conceptual diagram of the EI framework is shown in Fig. 1, with its training algorithm given in Sec. 3.5.

3.1. [INT] Token Generation

For each reference modality, indexed by $r \in R$, we use an auxiliary VFM $\phi_{a,r}$ to generate its [INT] token. Current VFMs, *e.g.* CLIP [15] and DINOv2 [14], are Vision Transformers (ViT) based. A ViT with L transformer layers starts with a `conv` layer (Conv) that encodes an input image to a sequence of patch-level tokens Z^0 . Prepend with a special [CLS] token, Z^0 is then fed into the stacked transformers, layer by layer, to progressively yield higher-level semantic tokens. For the ease of reference, we denote the output of the l -th transformer layer¹ as $Z^l = \phi(Z^0, l)$, with the corresponding [CLS] token accessed via $Z^l[0]$.

Under the hypothesis that the [CLS] token from the final transformer layer best represents the reference modality’s semantics, we use it as the [INT] token. For the multiple references R , we collect their [CLS] tokens as $\text{CLS}_{a,R}$. As these tokens are designed to intervene in the target modality’s feature extraction at an early stage, an adapter is necessary to enhance their compatibility. More formally, the [INT] token sequence is generated as

$$\begin{cases} \text{CLS}_{a,R} & \leftarrow \{\phi_{a,r}(\text{Conv}(\mathbf{x}[r]), L)[0] \mid r \in R\}, \\ \text{INT} & \leftarrow \text{Adapter}(\text{CLS}_{a,R}). \end{cases} \quad (1)$$

We use a two-layer MLP as the adapter.

3.2. Primary Feature Extraction with [INT]

For the current target modality (t), we use a primary VFM $\phi_{p,t}$ to extract features for classification. In order to leverage the [INT] token sequence at the very beginning of primary feature extraction, we concatenate the sequence with the output of the conv layer, namely Z_t^0 , forming \hat{Z}_t^0 . Using \hat{Z}_t^0 instead of Z_t^0 for subsequent forward computation in $\phi_{p,t}$ allows [INT] to interact with and thus influence the target-modality tokens at all layers, ultimately yielding an [INT]-intervened CLS token $\hat{\text{CLS}}_t$. The use of [INT] for

¹To simplify our notation, we omit position embedding.

primary feature extraction is expressed as

$$\begin{cases} \hat{Z}_t^0 & \leftarrow \text{Concat}(\text{Conv}(\mathbf{x}[t]), \text{INT}), \\ \hat{\text{CLS}}_t & \leftarrow \phi_{p,t}(\hat{Z}_t^0, L)[0]. \end{cases} \quad (2)$$

Executing Eq. (2) for each modality yields a set of multimodal feature as $\{\hat{\text{CLS}}_1, \dots, \hat{\text{CLS}}_M\}$. These features will be used for classification (Sec. 3.3).

3.3. Adaptive Late Fusion

As shown in Fig. 1, we use a lightweight fusion module that aggregates the multimodal features in an adaptive manner. In particular, each modality-specific feature $\hat{\text{CLS}}_t$ is projected into a C -dimensional vector \hat{y}_t by a linear layer. A gating layer, composed of a linear layer followed by `softmax`, generates an M -dimensional weight vector $\{\alpha_1, \dots, \alpha_M\}$, representing the importance of each modality. The final prediction \hat{y} is then computed as a weighted combination of the modality-specific predictions, see Eq. (3).

$$\begin{cases} \{\hat{y}_1, \dots, \hat{y}_M\} & \leftarrow \{\text{Linear}(\hat{\text{CLS}}_t) \mid t = 1, \dots, M\}, \\ \{\alpha_1, \dots, \alpha_M\} & \leftarrow \text{Gating}(\{\hat{\text{CLS}}_t\}), \\ \hat{y} & \leftarrow \sum_{t=1}^M \alpha_t \hat{y}_t. \end{cases} \quad (3)$$

We use \hat{y} at the inference stage.

3.4. MoR for Parameter-Efficient VFM Adaptation

For parameter-efficient VFM adaptation, we improve over LoRA [4] and its MoE variant [3] with the proposed Mixture of Low-varied-Ranks Adaptation (MoR). As illustrated in Fig. 3, MoR has two novel designs as follows.

First, **adaptive rank selection**. Based on our observation that the optimal choice of the rank used in a LoRA module varies over modalities and instances, we leverage multiple LoRA modules, each with a distinct rank, instead of a fixed-value rank (typically 4). In this work, we use three ranks: 2, 4 and 8. A router (`linear plus softmax`) is then used for adaptive rank selection.

Second, **a relaxed router with a bypass**. Note that A standard MoE router constrains its output weights to sum to unity [5], enforcing LoRAMoE to accept the adaptation even when the original weights are better. We fix the issue with a simple *bypass* trick. Specifically, by increasing the output dimension of the router from 3 to 4, we create a bypass pathway that enables the module to (partially) accept or reject the outputs of the individual LoRAs. In the extreme case where the bypass weight (w_0 in Fig. 3) is projected to be 1, the adaptation will be entirely skipped.

Following the typical use of LoRA, our MoR is also applied to the `linear` layers in the VFMs. For a given linear layer with a frozen weight matrix $W \in \mathbb{R}^{d \times d}$, let h and h' denote its input and output, respectively. As previously

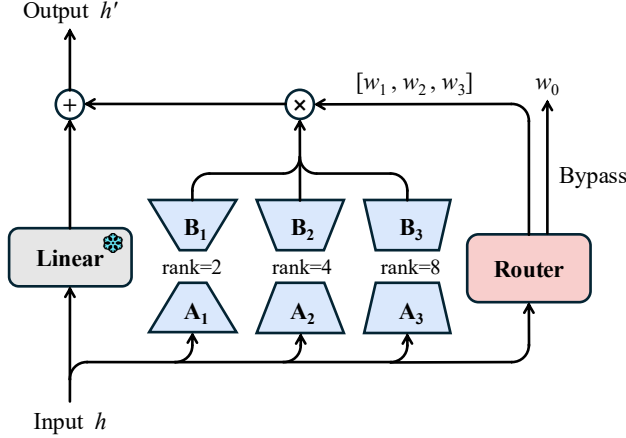


Figure 3. **Proposed Mixture of Low-varied-Ranks Adaptation (MoR) method for parameter-efficient VFM adaptation.** Compared to LoRA [4] and LoRAMoE [3], MoR has two novel designs: 1) multiple LoRAs with *distinct* ranks instead of a fixed-value rank, and 2) a relaxed router with a *bypass* to adaptively accept or reject the adaptation per instance.

stated, the MoR consists of three LoRAs. Each LoRA, assigned with a distinct rank r_k , is parameterized by matrices $A_k \in \mathbb{R}^{r_k \times d}$ and $B_k \in \mathbb{R}^{d \times r_k}$, and yields an output as $B_k A_k h$. The adapted version of h' is obtained by combining the outputs of the LoRAs as follows:

$$\begin{cases} [w_0, w_1, w_2, w_3] \leftarrow \text{Router}(h), \\ h' \leftarrow Wh + \sum_{k=1}^3 w_k B_k A_k h. \end{cases} \quad (4)$$

3.5. Training Algorithm

Primary Loss. Given the modality-specific predictions $\{\hat{y}_t\}$ and the multimodal prediction \hat{y} calculated by Eq. (3), we define our primary loss \mathcal{L}_p as the sum of the standard cross-entropy (CE) loss per prediction:

$$\mathcal{L}_p = \text{CE}(y, \hat{y}) + \sum_{t=1}^M \text{CE}(y, \hat{y}_t). \quad (5)$$

Auxiliary Loss for the Auxiliary VFMs. In order to supervise the auxiliary VFMs $\{\phi_{a,1}, \dots, \phi_{a,M}\}$ to generate task-related [INT] tokens, we add a linear classification head to each ϕ_a . Denoting the output as \hat{y}_a , we define an auxiliary loss w.r.t. the auxiliary VFMs \mathcal{L}_{aa} as

$$\begin{cases} \text{CLS}_{a,i} \leftarrow \phi_{a,i}(\text{Conv}(\mathbf{x}[i]), L)[0], \\ \hat{y}_{a,i} \leftarrow \text{Linear}(\text{CLS}_{a,i}), \\ \mathcal{L}_{aa} \leftarrow \sum_{i=1}^M \text{CE}(y, \hat{y}_{a,i}). \end{cases} \quad (6)$$

Auxiliary Loss for the Gating Layer. Ideally, the gating module as defined in Eq. (3) should learn to produce optimal weights for late fusion. Empirically, however, we find

that the VFM-based framework tends to overfit the training data, causing the modality-specific VFMs to saturate and perform equally well in the training stage. This saturation obscures their true performance differences, making it difficult for the gating network to discern which VFM is genuinely better. To alleviate the issue, we introduce a modality-wise prior π , derived from the best-performing modality on the training set, to supervise the gating layer. Specifically, π is a one-hot vector indicating the winning modality. We thus define an auxiliary gating loss \mathcal{L}_{ag} as:

$$\mathcal{L}_{ag} = \text{CE}(\pi, \{\alpha_1, \dots, \alpha_M\}). \quad (7)$$

The EI network is trained to minimize a joint loss as

$$\mathcal{L}_p + \lambda_1 \mathcal{L}_{aa} + \lambda_2 \mathcal{L}_{ag}, \quad (8)$$

where λ_1 and λ_2 are hyper-parameters empirically set to 0.3 and 0.1 respectively for all datasets, see a sensitivity analysis in Sec. 4.3.3. The training procedure is summarized in Algorithm 1.

4. Experiments

4.1. Experimental Setup

Datasets. We adopt three public medical image datasets corresponding to three distinct organs:

- **MMC-AMD [17]**: Four-class Age-related Macular Degeneration (AMD) classification, *i.e.* *dry AMD*, *wet AMD*, *PCV* and *normal*. Each multimodal sample consists of a CFP image and an OCT image.
- **Derm7pt [7]**: Five-class skin lesion recognition, *i.e.* *basal cell carcinoma (BCC)*, *nevus (NEV)*, *melanoma (MEL)*, *seborrheic keratosis (SK)* and *miscellaneous (MISC)*. Each multimodal sample consists of a dermoscopic image and a clinic image.
- **MRNet [1]**: Multi-label knee abnormality classification, *i.e.* *abnormal*, *anterior cruciate ligament (ACL) tear* and *meniscal tear*. Each multimodal sample consists of MRI images from sagittal-view, axial-view and coronal-view.

For MMC-AMD and Derm7pt, we use their official data splits. As for MRNet, since only the training and validation sets are publicly available, we use the validation set as our test set, whilst selecting at random 120 samples from the training set as a held-out validation set. An overview of the datasets is given in Tab. 2. See visual examples in Fig. 2.

Evaluation Criteria. We adopt Average Precision (AP) as the primary performance metric. In addition, we report AUC and the harmonic mean of sensitivity and specificity (S2) as secondary metrics. Each metric is computed per class. The overall performance per dataset is obtained by averaging over the classes, denoted as mAP, mAUC and mS2, respectively. Unless otherwise stated, we report AP and mAP, with the other metrics given in the supplement.

Algorithm 1: EI in a PyTorch style

```
1 Input: Multimodal training_set D={(x,y)},
2       VFM phi,
3       Modality prior pi
4 Output: Trained EI network
5
6 L = 12
7 MoR_a, MoR_p = [MoR]*M, [MoR]*M
8 phi.requires_grad = False
9 EI = [MoR_a, MoR_p, adapter, linear, ...]
10 optimizer = SGD(EI.parameters)
11 # Show only one training epoch
12 for mini-batch {(x, y)} in D:
13     optimizer.zero_grad()
14     # Extract [CLS] by the auxiliary VFMs
15     cls_a = [0]*M
16     for t in range(M):
17         phi_a = phi, MoR_a[t]
18         cls_a[t] = phi_a(conv(x[t]), L) [0]
19     # Early intervention
20     cls_p = [0]*M
21     for t in range(M):
22         R = [r for r in range(M) if r!=t]
23         INT = [adapter(cls_a[r]) for r in R]
24         Z_0 = concat(conv(x[t]), INT)
25         phi_p = phi, MoR_p[t]
26         cls_p[t] = phi_p(Z_0, L) [0]
27     # Adaptive late fusion
28     hat_yp = linear(cls_p)
29     alpha = gating(cls_p)
30     hat_y = torch.dot(alpha, hat_yp)
31     loss_p = ce(y, hat_y) + ce(y, hat_yp)
32     loss_aa = ce(y, linear(cls_a))
33     loss_ag = ce(pi, alpha)
34     loss = loss_p+0.3*loss_aa+0.1*loss_ag
35     loss.backward()
36     optimizer.step()
```

Table 2. Three medical image datasets used in our evaluation.

Dataset	Organ	M	C	#Multimodal samples			
				Total	Train	Val.	Test
MMC-AMD[17]	eye	2	4	768	610	79	79
Derm7pt[7]	skin	2	5	1,011	413	203	395
MRNet[1]	knee	3	3	1,250	1,010	120	120

Choice of VFMs. We adopt two generic VFMs: CLIP(ViT-B/16) [15] and DINOv2(ViT-B/14) [14]. See Sec. 4.3.2 for a comparison to domain-specific counterparts.

Details of Implementation. The input image resolutions were set according to the official recommendations for each dataset: 448*448 for MMC-AMD, 512*512 for Derm7pt, and 256*256 for MRNet. Per 3D-volume sample in MRNet, we select four slices, which are sampled at ran-

dom during training and sampled uniformly for inference, respectively. A sample-level feature is obtained by mean pooling over the selected slices.

We use the following training protocol. The network optimizer is SGD with a momentum of 0.95 and a weight decay of 1e-4. The learning rate scheduler is CyclicLR (cycling between 1e-5 and 1e-3) combined with a warmup strategy. Batch size is set to 8. Validation is performed every epoch. Early stop occurs if there is no performance increase in 10 successive validations. For each modality we initialize its auxiliary and primary VFMs using a model pre-adapted with MoR on the unimodal training data. All experiments were conducted using PyTorch 3.12 on four NVIDIA GeForce RTX 4090 GPUs.

4.2. EI versus Previous Multimodal Methods

Baselines. To ensure reproducibility, we selected baseline methods that are open-source or have publicly accessible code. Furthermore, since our evaluation involves medical image classification tasks from distinct domains, the chosen baselines must be applicable with minimal adjustment. Accordingly, we have compiled a list of six baselines, put into three groups based on their feature fusion strategies:

- Group I. *Concatenation*: CosCat [25] and DynMM [19].
- Group II. *Weighted summation*: MM-MIL [10] and SFusion [11].
- Group III. *Attention based*: RadDiag [23] and MM-RAD [9].

Note that for a fair comparison, for all the baselines we replace their original visual backbones by the VFMs. We also follow their own setups, having the backbones either frozen (as in MMRAD which uses prompt learning) or full-parameter fine-tuned (as in the rest). See Tab. 3 for the amount of trainable parameters per baseline.

Enhanced Baselines. To enable a more conclusive comparison, we enhance MM-MIL and MMRAD by adapting their VFMs with our MoR method. We refer to these enhanced versions as **MM-MIL-MoR** and **MMRAD-MoR**, respectively. Furthermore, to investigate the necessity of modality-specific VFMs, we construct a single-VFM baseline named **UniModel**. In this model, patch tokens extracted from multi-modal images are merged into a unified input sequence.

Results. Tab. 3 shows the per-dataset, per-class and overall results of the different multimodal methods. Among the six baselines, MMRAD is the best, confirming our hypothesis that PEFT is crucial for VFM-based medical image classification where multimodal training samples are in relatively short supply. The proposed EI outperforms MMRAD by a large margin in light of the overall performance, *i.e.* 0.729 \rightarrow 0.824 with CLIP as VFM and 0.735 \rightarrow 0.841 with DINOv2 as VFM. Its superior performance is also consistently observed across datasets.

Table 3. **Comparison of multimodal methods across three datasets.** Baselines are sorted in ascending order by their MEAN performance. The amount of trainable parameters per method is averaged over the datasets.

Method	Params. (M)	MEAN	MMC-AMD					Derm7pt					MRNet				
			mAP	Normal	dryAMD	PCV	wetAMD	mAP	BCC	NEV	MEL	SK	MISC	mAP	Abnormal	Meniscal	ACL
VFM: CLIP																	
RadDiag	212.2	0.648	0.783	1.0	0.922	0.659	0.551	0.352	0.128	0.756	0.480	0.068	0.327	0.809	0.954	0.652	0.822
DynMM	402.2	0.671	0.830	1.0	0.928	0.810	0.580	0.349	0.148	0.767	0.422	0.063	0.345	0.833	0.958	0.696	0.846
MM-MIL	202.5	0.671	0.818	1.0	0.919	0.761	0.592	0.360	0.105	0.782	0.441	0.075	0.396	0.835	0.972	0.674	0.858
CosCat	201.0	0.679	0.839	1.0	0.929	0.826	0.602	0.364	0.163	0.775	0.493	0.080	0.309	0.835	0.974	0.685	0.845
SFusion	263.4	0.683	0.840	1.0	0.946	0.754	0.662	0.375	0.158	0.737	0.523	0.067	0.391	0.835	0.976	0.673	0.856
MMRAD	9.3	0.729	0.819	1.0	0.928	0.684	0.664	0.549	0.421	0.879	0.510	0.345	0.590	0.818	0.959	0.679	0.815
EI	8.9	0.824	0.889	1.0	0.880	0.896	0.782	0.721	0.577	0.928	0.758	0.647	0.694	0.861	0.973	0.748	0.863
MM-MIL-MoR	5.0	0.793	0.879	1.0	0.913	0.893	0.710	0.651	0.451	0.926	0.718	0.504	0.659	0.850	0.976	0.735	0.838
MMRAD-MoR	12.5	0.783	0.865	1.0	0.802	0.956	0.701	0.651	0.437	0.937	0.677	0.582	0.623	0.833	0.969	0.696	0.834
UniModel	1.5	0.740	0.868	1.0	0.933	0.835	0.706	0.548	0.370	0.907	0.628	0.214	0.618	0.803	0.973	0.668	0.767
VFM: DINOv2																	
SFusion	265.8	0.687	0.821	1.0	0.915	0.678	0.690	0.401	0.208	0.821	0.462	0.077	0.438	0.839	0.972	0.720	0.826
DynMM	404.3	0.688	0.854	1.0	0.933	0.782	0.701	0.377	0.183	0.813	0.427	0.068	0.395	0.833	0.970	0.689	0.839
CosCat	202.0	0.693	0.823	1.0	0.931	0.767	0.594	0.417	0.267	0.836	0.447	0.081	0.451	0.841	0.973	0.693	0.856
RadDiag	213.3	0.717	0.826	1.0	0.935	0.708	0.662	0.499	0.365	0.847	0.554	0.182	0.549	0.825	0.962	0.691	0.822
MM-MIL	203.6	0.733	0.863	1.0	0.932	0.861	0.658	0.502	0.406	0.867	0.561	0.170	0.507	0.835	0.972	0.707	0.826
MMRAD	9.3	0.735	0.821	1.0	0.919	0.789	0.576	0.566	0.437	0.879	0.521	0.446	0.546	0.818	0.968	0.705	0.781
EI	8.9	0.841	0.909	1.0	0.916	0.929	0.789	0.767	0.690	0.932	0.755	0.777	0.682	0.848	0.978	0.734	0.833
MM-MIL-MoR	5.0	0.823	0.906	1.0	0.908	0.929	0.787	0.724	0.578	0.931	0.764	0.756	0.592	0.837	0.968	0.741	0.803
MMRAD-MoR	12.5	0.806	0.901	1.0	0.879	0.931	0.795	0.687	0.558	0.923	0.722	0.683	0.547	0.829	0.966	0.708	0.813
UniModel	1.5	0.770	0.883	1.0	0.899	0.906	0.725	0.615	0.519	0.903	0.618	0.520	0.516	0.812	0.972	0.673	0.792

When comparing the three tasks, all the methods perform relatively lower on Derm7pt (skin lesion recognition), suggesting a large domain gap between the two generic VFMs and the dermoscopic and clinic images. Nevertheless, EI achieves the largest gain over the best baseline (MMRAD) in this task. Since both methods have a similar number of trainable parameters, this outcome confirms the efficacy of EI in harnessing VFMs across large domain gaps.

The superior performance of MM-MIL-MoR and MMRAD-MoR over their original counterparts shows that MoR is more effective than both full-parameter tuning (used in MM-MIL) and prompt learning (used in MMRAD). Since these enhanced baselines and UniModel also employ MoR, the fact that EI outperforms them confirms the distinct advantage of our proposed early intervention strategy.

4.3. Ablation Studies

4.3.1. Choices of [INT] Token Acquisition and Usage

By default, per reference modality, we acquire its [INT] token from the last [CLS] token of its auxiliary VFM (Sec. 3.1), and insert [INT] into the input of the first Transformer layer of the target modality’s primary VFM (Sec. 3.2). As Tab. 4 shows, while the optimal layer for [INT] acquisition depends on the VFM in use, *i.e.* 12 for CLIP and 3 for DINOv2, the last layer is the best on average. For both VFMs, inserting [INT] at Layer 0, which is the earliest possible point, yields the best performance. This result clearly justifies the early intervention principle.

4.3.2. Generic or Specialized VFMs?

Domain-specific VFMs. We compare with three domain-specific VFMs: RETFound [24] for fundus images, PanDerm [20] for skin images, and RadioDINO [22] for radio-

Table 4. **Evaluating the choices of [INT] acquisition and usage.**

Layer	to acquire [INT]			Layer	to use [INT]		
	CLIP	DINOv2	Average		CLIP	DINOv2	Average
1	0.818	0.836	0.827	0	0.824	0.841	0.833
2	0.811	0.832	0.822	1	0.818	0.835	0.826
3	0.806	0.846	0.826	2	0.814	0.823	0.819
4	0.813	0.837	0.825	3	0.821	0.830	0.825
5	0.810	0.835	0.822	4	0.817	0.817	0.817
6	0.805	0.833	0.819	5	0.815	0.829	0.822
7	0.815	0.841	0.828	6	0.811	0.822	0.816
8	0.818	0.836	0.827	7	0.804	0.822	0.813
9	0.803	0.838	0.820	8	0.798	0.828	0.813
10	0.808	0.841	0.824	9	0.810	0.825	0.817
11	0.814	0.845	0.830	10	0.807	0.815	0.811
12	0.824	0.841	0.833	11	0.808	0.822	0.815

logical images. Each model is used in the EI framework for its corresponding task: RETFound for MMC-AMD, PanDerm for Derm7pt, and RadioDINO for MRNet. To ensure a fair comparison, we use the ViT-B/16 versions where available. An exception is RETFound, for which only a larger ViT-L/14 version is provided. As a larger VFM typically yields better performance, such model size discrepancy may confer a performance advantage to RETFound.

Results. As shown in Tab. 5, the three specialized VFMs are inferior to their generic counterparts. We attribute this to the richer feature representations and superior generalization capability of generic VFMs. In light of substantial resources required to develop domain-specific models, our finding suggests that effectively adapting generic VFMs is more efficient and promising.

4.3.3. The Impact of the Auxiliary Losses

To investigate the impact of the auxiliary losses \mathcal{L}_{aa} and \mathcal{L}_{ag} , we conduct a sensitivity analysis by varying their re-

Table 5. Specialized *versus* generic VFMs.

VFM	Params.(M)	mAP	mAUC	mS2
Dataset: MMC-AMD				
RETFound [24]	17.3	0.800	0.914	0.800
CLIP	7.1	0.889	0.958	0.830
DINOv2	7.1	0.909	0.959	0.887
Dataset: Derm7pt				
PanDerm [20]	7.1	0.589	0.886	0.707
CLIP	7.1	0.721	0.929	0.742
DINOv2	7.1	0.767	0.932	0.790
Dataset: MRNet				
RadioDINO [22]	12.4	0.818	0.844	0.563
CLIP	12.4	0.861	0.869	0.725
DINOv2	12.4	0.848	0.860	0.704

Table 6. Influence of the auxiliary losses: $\mathcal{L}_{aa}(\lambda_1)$ and $\mathcal{L}_{ag}(\lambda_2)$. Default choice ($\lambda_1=0.3$, $\lambda_2=0.1$) is shown in color.

λ_1	CLIP	DINOv2	Average	λ_2	CLIP	DINOv2	Average
0.0	0.807	0.834	0.820	0.0	0.791	0.831	0.811
0.1	0.816	0.840	0.828	0.1	0.824	0.841	0.833
0.2	0.820	0.839	0.829	0.2	0.810	0.838	0.824
0.3	0.824	0.841	0.833	0.3	0.811	0.844	0.828
0.4	0.821	0.834	0.827	0.4	0.811	0.835	0.823
0.5	0.803	0.836	0.820	0.5	0.810	0.838	0.824
0.6	0.807	0.831	0.819	0.6	0.808	0.828	0.818
0.7	0.822	0.819	0.820	0.7	0.810	0.833	0.822
0.8	0.814	0.836	0.825	0.8	0.805	0.832	0.819
0.9	0.808	0.835	0.822	0.9	0.810	0.836	0.823
1.0	0.807	0.843	0.825	1.0	0.815	0.833	0.824

spective weights (λ_1 and λ_2) one at a time. We set $\lambda_1 = 0.3$ when varying λ_2 , and $\lambda_2 = 0.1$ when varying λ_1 . As shown in Tab. 6, disabling either auxiliary loss (by setting its corresponding weight to zero) results in a clear degradation of the MEAN performance.

4.3.4. MoR *versus* Others for VFM Adaptation

Unimodal Image Classification. We start with the unimodal setting. We compare MoR against several representative PEFT methods: VPT [6], RLRR [2], BitFit [21], LoRA [4], LoSA [13] and LoRAMoE [3]. We also include LateLoRA [16], more recently developed for medical image analysis. For broader context, we include Full-Parameter Tuning (FPT) to assess the necessity of PEFT, and Linear Probing (LP) to establish a minimal-tuning baseline. As shown in Tab. 7, FPT and LP are the weakest, underscoring the need of advanced PEFT. Among the established PEFT baselines, LoRAMoE is the best. The proposed MoR consistently surpasses LoRAMoE. The benefit of the bypass is also confirmed, as its removal from MoR leads to consistent performance degradation across all datasets.

Multimodal Image Classification. We evaluate LoRA and LoRAMoE within the EI framework. In addition, we report the result of using a completely frozen VFM without any adaptation. MoR is again the best, see Tab. 8.

Table 7. MoR *versus* previous VFM adaptation methods for **unimodal image classification**. Baselines are sorted in ascending order by their MEAN performance.

Method	Params.(K)	MEAN	MMC-AMD	Derm7pt	MRNet
VFM: CLIP					
FPT	86,180	0.574	0.681	0.315	0.727
LP	3	0.610	0.682	0.413	0.734
VPT[6]	49	0.616	0.678	0.425	0.745
LoSA[13]	100	0.626	0.698	0.426	0.753
LateLoRA[16]	77	0.689	0.770	0.504	0.792
LoRA[4]	372	0.700	0.784	0.510	0.805
BitFit[21]	106	0.705	0.808	0.498	0.809
RLRR[2]	292	0.707	0.804	0.504	0.813
LoRAMoE[3]	1,247	0.713	0.788	0.544	0.806
MoR	1,478	0.737	0.820	0.576	0.816
MoR <i>w/o</i> bypass	1,432	0.730	0.807	0.569	0.814
VFM: DINO-v2					
FPT	86,587	0.622	0.755	0.335	0.775
LP	3	0.665	0.733	0.518	0.743
LoSA	113	0.666	0.745	0.511	0.742
VPT	49	0.679	0.776	0.471	0.790
LateLoRA	77	0.720	0.782	0.598	0.779
BitFit	106	0.723	0.803	0.572	0.794
RLRR	292	0.724	0.810	0.567	0.795
LoRAMoE	1,247	0.724	0.796	0.591	0.786
LoRA	372	0.725	0.811	0.579	0.785
MoR	1,478	0.740	0.823	0.601	0.795
MoR <i>w/o</i> bypass	1,432	0.735	0.817	0.595	0.793

Table 8. MoR *versus* Alternatives within the EI framework.

Method	Params.(M)	MEAN	MMC-AMD	Derm7pt	MRNet
VFM: CLIP					
Frozen	2.0	0.647	0.725	0.420	0.763
LoRA	2.7	0.786	0.884	0.617	0.856
LoRAMoE	7.8	0.788	0.861	0.651	0.853
MoR	8.9	0.824	0.889	0.721	0.861
VFM: DINOv2					
Frozen	2.0	0.710	0.816	0.576	0.737
LoRA	2.7	0.810	0.870	0.727	0.834
LoRAMoE	7.8	0.830	0.886	0.763	0.841
MoR	8.9	0.841	0.909	0.767	0.848

5. Conclusions

The proposed EI framework has effectively addressed two major challenges in multimodal medical image classification: 1) the information bottleneck due to the delayed fusion paradigm, limiting the full utilization of multimodal data, and 2) the inapplicability of cutting-edge VFMs due to their large domain gap to medical imagery. Extensive experiments on three public datasets verify the efficacy of our framework, yielding key findings as follows. The optimal strategy for acquiring the [INT] tokens is to use the final [CLS] tokens from reference modalities. Inserting [INT] before the first Transformer layer of the target VFM is the best. Generic VFMs, when properly adapted, outperform their domain-specific counterparts. Both the early intervention strategy and the MoR module are crucial to EI’s superior performance, as confirmed by ablation studies.

Limitations. The acquisition and insertion points for the [INT] tokens are fixed. An adaptive positioning mechanism may enhance performance further. Concerning [INT] token generation, the feasibility of replacing auxiliary VFM with more lightweight networks warrants further investigation.

Acknowledgments. This research was supported by Beijing Natural Science Foundation (L254039) and National Natural Science Foundation of China (62576348)

References

- [1] Nicholas Bien, Pranav Rajpurkar, Robyn L Ball, Jeremy Irvin, Allison Park, Erik Jones, Michael Bereket, Bhavik N Patel, Kristen W Yeom, Katie Shpanskaya, et al. Deep-learning-assisted diagnosis for knee magnetic resonance imaging: Development and retrospective validation of MR-Net. *PLoS medicine*, 15(11):e1002699, 2018. 2, 3, 5, 6
- [2] Wei Dong, Xing Zhang, Bihui Chen, Dawei Yan, Zhijun Lin, Qingsen Yan, Peng Wang, and Yang Yang. Low-rank rescaled vision transformer fine-tuning: A residual design approach. In *CVPR*, 2024. 3, 8
- [3] Shihan Dou, Enyu Zhou, Yan Liu, Songyang Gao, Wei Shen, Limao Xiong, Yuhao Zhou, Xiao Wang, Zhiheng Xi, Xiaoran Fan, et al. LoRAMoE: Alleviating world knowledge forgetting in large language models via MoE-style plugin. In *ACL*, 2024. 3, 4, 5, 8
- [4] Edward J Hu, Yelong Shen, Phillip Wallis, Zeyuan Allen-Zhu, Yuanzhi Li, Shean Wang, Lu Wang, Weizhu Chen, et al. LoRA: Low-rank adaptation of large language models. In *ICLR*, 2022. 3, 4, 5, 8
- [5] Robert A Jacobs, Michael I Jordan, Steven J Nowlan, and Geoffrey E Hinton. Adaptive mixtures of local experts. *Neural computation*, 3(1):79–87, 1991. 4
- [6] Menglin Jia, Luming Tang, Bor-Chun Chen, Claire Cardie, Serge Belongie, Bharath Hariharan, and Ser-Nam Lim. Visual prompt tuning. In *ECCV*, 2022. 3, 8
- [7] Jeremy Kawahara, Sara Daneshvar, Giuseppe Argenziano, and Ghassan Hamarneh. Seven-point checklist and skin lesion classification using multitask multimodal neural nets. *Journal of Biomedical and Health Informatics*, 23(2):538–546, 2018. 2, 3, 5, 6
- [8] Sachin Kumar, Sita Rani, Shivani Sharma, and Hong Min. Multimodality fusion aspects of medical diagnosis: A comprehensive review. *Bioengineering*, 11(12):1233, 2024. 1
- [9] Jingtao Li, Ting Chen, Xinyu Wang, Yanfei Zhong, and Xuan Xiao. Adapting the segment anything model for multimodal retinal anomaly detection and localization. *Information Fusion*, 113:102631, 2025. 2, 3, 6
- [10] Xirong Li, Yang Zhou, Jie Wang, Hailan Lin, Jianchun Zhao, Dayong Ding, Weihong Yu, and Youxin Chen. Multi-modal multi-instance learning for retinal disease recognition. In *ACM MM*, 2021. 2, 3, 6
- [11] Zecheng Liu, Jia Wei, Rui Li, and Jianlong Zhou. SFusion: Self-attention based n-to-one multimodal fusion block. In *MICCAI*, 2023. 2, 3, 6
- [12] Zheda Mai, Ping Zhang, Cheng-Hao Tu, Hong-You Chen, Quang-Huy Nguyen, Li Zhang, and Wei-Lun Chao. Lessons and insights from a unifying study of parameter-efficient fine-tuning (PEFT) in visual recognition. In *CVPR*, 2025. 3
- [13] Otniel-Bogdan Mercea, Alexey Gritsenko, Cordelia Schmid, and Anurag Arnab. Time-, memory- and parameter-efficient visual adaptation. In *CVPR*, 2024. 3, 8
- [14] Maxime Oquab, Timothée Darcet, Théo Moutakanni, Huy Vo, Marc Szafraniec, Vasil Khalidov, Pierre Fernandez, Daniel Haziza, Francisco Massa, Alaaeldin El-Nouby, et al. DINOv2: Learning robust visual features without supervision. *Transactions on Machine Learning Research Journal*, pages 1–31, 2024. 2, 4, 6
- [15] Alec Radford, Jong Wook Kim, Chris Hallacy, Aditya Ramesh, Gabriel Goh, Sandhini Agarwal, Girish Sastry, Amanda Askell, Pamela Mishkin, Jack Clark, et al. Learning transferable visual models from natural language supervision. In *ICML*, 2021. 2, 4, 6
- [16] Carolin Teuber, Anwai Archit, and Constantin Pape. Parameter efficient fine-tuning of segment anything model for biomedical imaging. In *MIDL*, 2025. 8
- [17] Weisen Wang, Xirong Li, Zhiyan Xu, Weihong Yu, Jianchun Zhao, Dayong Ding, and Youxin Chen. Learning two-stream CNN for multi-modal age-related macular degeneration categorization. *Journal of Biomedical and Health Informatics*, 26(8):4111–4122, 2022. 2, 3, 5, 6
- [18] Yan Wang, Liangli Zhen, Tien-En Tan, Huazhu Fu, Yangqin Feng, Zizhou Wang, Xinxing Xu, Rick Siow Mong Goh, Yipin Ng, Claire Calhoun, et al. Geometric correspondence-based multimodal learning for ophthalmic image analysis. *IEEE Transactions on Medical Imaging*, 43(5):1945–1957, 2024. 2, 3
- [19] Zihui Xue and Radu Marculescu. Dynamic multimodal fusion. In *CVPRW*, 2023. 6
- [20] Siyuan Yan, Zhen Yu, Clare Primiero, Cristina Vico-Alonso, Zhonghua Wang, Litao Yang, Philipp Tschandl, Ming Hu, Lie Ju, Gin Tan, et al. A multimodal vision foundation model for clinical dermatology. *Nature Medicine*, pages 1–12, 2025. 7, 8
- [21] Elad Ben Zaken, Yoav Goldberg, and Shauli Ravfogel. Bit-Fit: Simple parameter-efficient fine-tuning for transformer-based masked language-models. In *ACL*, 2022. 3, 8
- [22] Luca Zedda, Andrea Loddo, and Cecilia Di Ruberto. Radio DINO: A foundation model for advanced radiomics and AI-driven medical imaging analysis. *Computers in Biology and Medicine*, 195:110583, 2025. 7, 8
- [23] Qiaoyu Zheng, Weike Zhao, Chaoyi Wu, Xiaoman Zhang, Lisong Dai, Hengyu Guan, Yuehua Li, Ya Zhang, Yanfeng Wang, and Weidi Xie. Large-scale long-tailed disease diagnosis on radiology images. *Nature Communications*, 15(1): 10147, 2024. 2, 3, 6
- [24] Yukun Zhou, Mark A Chia, Siegfried K Wagner, Murat S Ayhan, Dominic J Williamson, Robbert R Struyven, Timing Liu, Moucheng Xu, Mateo G Lozano, Peter Woodward-Court, et al. A foundation model for generalizable disease detection from retinal images. *Nature*, 622(7981):156–163, 2023. 7, 8
- [25] Lihan Zuo, Zizhou Wang, and Yan Wang. A multi-stage multi-modal learning algorithm with adaptive multimodal

fusion for improving multi-label skin lesion classification.
Artificial Intelligence in Medicine, 162:103091, 2025. [2](#), [3](#),
[6](#)